analytical chemistry

pubs.acs.org/ac Article

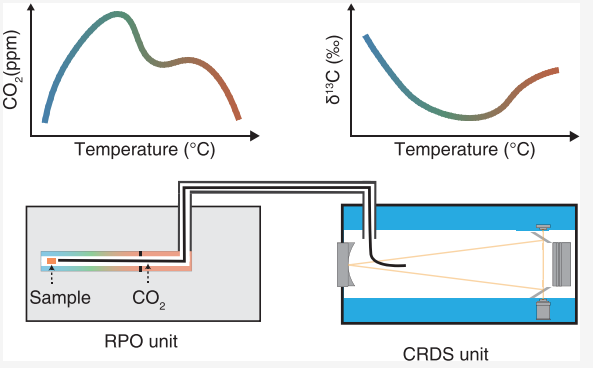
High-Resolution, Continuous Stable Carbon Isotope Analysis of Complex Organic Matter via Online Ramped Pyrolysis/Oxidation–Cavity Ring-Down Spectroscopy

Yipeng Wang, Mingzhi Liu, Yupeng Cao, Weiran Hu, Yekai Wang, Nan Wang, Longhai Zhu, and Rui Bao*

Cite This: https://doi.org/10.1021/acs.analchem.6c00100 Read Online

ACCESS | Metrics & More | Article Recommendations | Supporting Information

ABSTRACT: Sedimentary organic carbon (OC) is an important fraction of ocean carbon sinks and spans a broad reactivity continuum across heterogeneous mixtures. Stable carbon isotope ($\delta^{13}C$) measurements of bulk OC are widely used for source reconstruction, but they obscure isotopic heterogeneity among mixing OC components. Here, we couple ramped pyrolysis/oxidation (RPO) with cavity ring-down spectroscopy (CRDS) to enable continuous, online $\delta^{13}C$ measurements of CO_2 evolved during thermal decomposition, providing high-resolution temperature-$\delta^{13}C$ profiles for the concept of OC reactivity continuum. Analytical performance is evaluated via abundance-based signal thresholds, blank characterization, and $\delta^{13}C$ calibrations with international reference materials. Furthermore, we employed this system to resolve distinct $\delta^{13}C$ trajectories for labile, resistant, and refractory fractions of surface or core sediments in the East China Sea and Japan Trench, providing a new insight for source attribution across heterogeneous OC mixtures. The workflow can also be transferable to soils, aerosols, and other low-carbon matrices for mechanistic studies of carbon sources and stability in environmental and analytical chemistry.



Downloaded via OCEAN UNIV OF CHINA on May 14, 2026 at 12:23:54 (UTC).
See https://pubs.acs.org/sharingguidelines for options on how to legitimately share published articles.

Preservation of organic carbon (OC) in marine sediments is critical for quantifying ocean carbon sinks and their feedbacks on the global carbon cycle and climate[1,2] The extent of OC preservation depends on the source composition and stabilities of carbon input[3−5] and is continually modified by microbial transformation, mineral association, and physical transport.[6−10] Together, these inputs and processes drive sedimentary OC as a mixture spanning a broad continuum stability, ranging from labile to refractory components.[11−13] However, these recent conceptual advances, in understanding such complex organic mixtures as the OC reactivity continuum, have been limited by the corresponding stable isotope techniques, especially stable carbon isotope ($\delta^{13}C$) analysis, that are commonly bulk-averaged concept measurements.

Variations of the $\delta^{13}C$ value across OC mixtures are widely used to reconstruct sources and transformation processes from modern to paleorecords.[4,14−17] However, existing approaches treat sediments or a specific fraction as bulk materials for $\delta^{13}C$ values, obscuring heterogeneity within OC mixtures. For example, bulk $\delta^{13}C$ analysis by isotope ratio mass spectrometry (IRMS) converts heterogeneous organic matter (OM) to uniform CO_2 gas and reports a single integrated $\delta^{13}C$ value to trace OC sources and transformations.[14,18,19] In addition, for special molecules, compound-specific isotope analysis (CSIA) can resolve individual biomarkers, but it requires extensive separation and targets only a limited subset of compounds, potentially missing more information carried by the broader sedimentary OC mixture.[14,15] Thermal fractionation by ramped pyrolysis/oxidation (RPO) can separate OC by its continuum thermal reactivity,[20,21] but $\delta^{13}C$ analysis is often commonly the bulk OC measurement by IRMS, thereby masking isotopic heterogeneity across the OC continuum.[22−25] Consequently, the current bulk $\delta^{13}C$ measurement often does not fully reflect the advance that conceptualizes OC as a reactivity continuum, highlighting a methodological gap in performing higher resolution $\delta^{13}C$ analysis to characterize sources and stabilities of the OC continuum.[22,26,27]

The cavity ring-down spectroscopy (CRDS) technique has emerged as a robust alternative method for high-resolution $\delta^{13}C$ analysis in environmental applications.[28−30] Compared with IRMS, the minimal carbon requirements of CRDS are lower than 2−3 orders of magnitude (~0.5 to 5 ng C for 1 Hz) to

Received: January 12, 2026
Revised: April 25, 2026
Accepted: April 30, 2026

© XXXX American Chemical Society

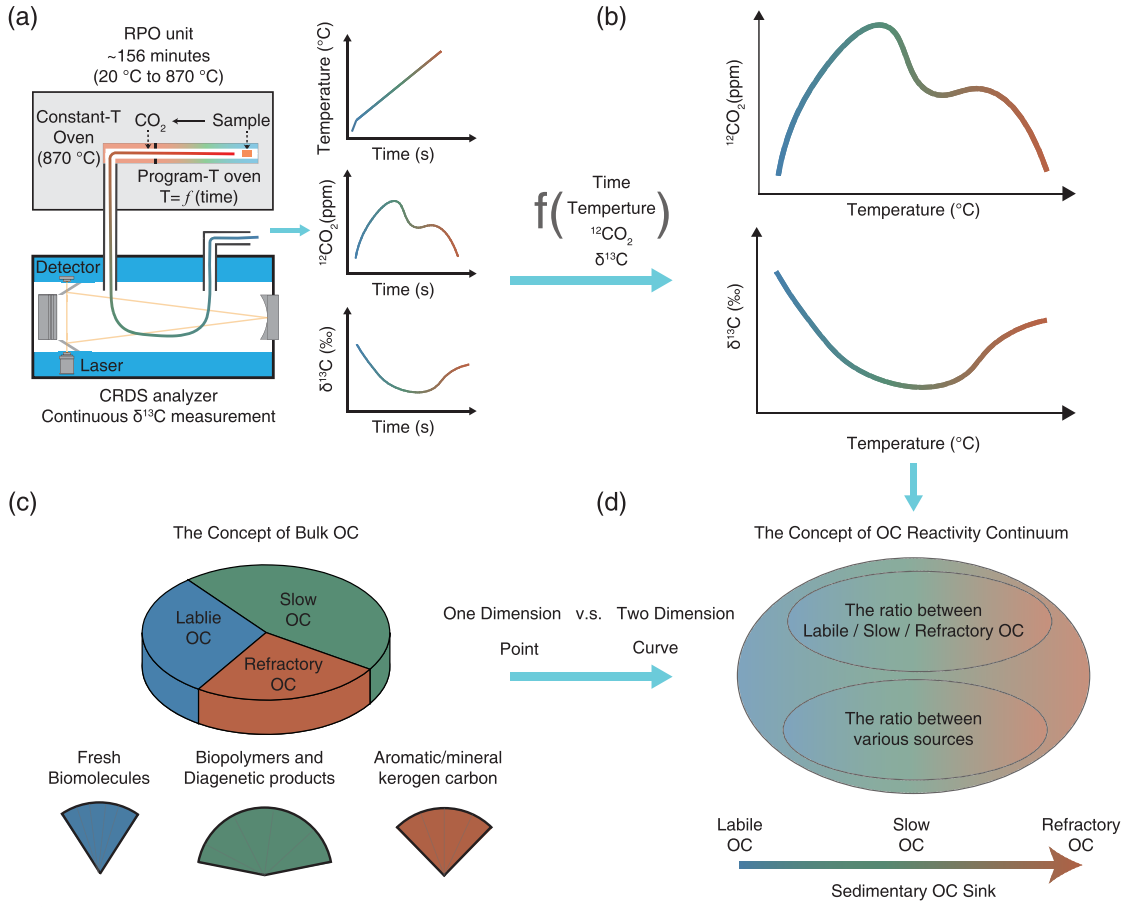


Figure 1. Conceptual overview of the RPO−CRDS system for marine OC sinks in marine sediments. OC in the marine sediment is illustrated as a mixture of labile, slow, and refractory pools associated, respectively, with fresh biomolecules, biopolymers and diagenetic products, and aromatic or mineral/kerogen-bound carbon.[6−10] (a) These sediments are combusted on quartz filters in an RPO unit with a programmable temperature oven and a constant-temperature oxidation oven, and the evolving gases are transferred to a CRDS analyzer. (b) Imposed temperature ramp produces distinct CO_2-release curves for the different reactivity classes, while the CRDS unit continuously measures CO_2 concentration and $\delta^{13}C$ as a function of time and temperature. (c, d) Integrating temperature-resolved CO_2 and $\delta^{13}C$ profiles allows us to quantify the relative contributions of labile, slow, and refractory OC within bulk sediments and to compare their partitioning with that of various ocean OC sinks for constraining the balance between OC sources, transformation, and long-term burial.

enable continuous, online $\delta^{13}C$ measurement.[31,32] Although its absolute accuracy (~0.15 to 0.5‰) is lower than that of IRMS (~0.02 to 0.05‰), CRDS is able to resolve isotopic variability across the typical ranges of natural OC (−10 to −40‰).[18,33] This advance of the CRDS technique in high-resolution $\delta^{13}C$ measurement is crucial for the concept of a sedimentary OC continuum. When integrated with RPO analysis, CRDS can provide point-by-point $\delta^{13}C$ values tracking across an entire thermogram, capturing the rapid isotopic shift among OC components that are commonly smoothed or obscured by bulk measurements but important for mechanistic interpretation of isotope fractionation with chemical reactivity.

Here, we develop an analytical system that couples a programmable RPO unit with a CRDS analyzer, to provide the high-resolution gap in the $\delta^{13}C$ characterization of complex organic matter. We further provide an abundance-based precision model to derive operational CO_2 thresholds that guide the carrier gas flow and sample mass selection, along with blank corrections and $\delta^{13}C$ calibration by international reference materials (IA-R006, IAEA-600, USGS-64). Finally, we demonstrate this system using marine sediments to obtain the first high-resolution $\delta^{13}C$ profile of the OC continuum, showing the inherent heterogeneity of sources and stability within a single marine sediment. This RPO-CRDS system expands $\delta^{13}C$ capabilities for tracing sources and constraining stabilities across environmental and geochemical matrices in analytical chemistry.

EXPERIMENTAL SECTION

Instrumentation

A schematic of the customized RPO-CRDS system is shown in Figure 1. The system comprises two modules coupled in sequence: (i) a custom RPO unit, spanning from room temperature to ~870 °C for quantitative conversion of sediment OC to CO_2 gas[34] and (ii) a CRDS analyzer for continuous, online determination of CO_2 concentration and $\delta^{13}C$ values.[35] The evolved gas stream from the RPO unit is transferred to the CRDS unit via copper tubing and carried under mass flow control by a fixed Ar/O_2 flow of 8 cc/min (5% O_2) together with a supplemental high-purity Ar flow (7−42 cc/min) at different flow settings. This sequential online configuration enables time-resolved acquisition (1 Hz) of $\delta^{13}C$ throughout the temperature program.

https://doi.org/10.1021/acs.analchem.6c00100
Anal. Chem. XXXX, XXX, XXX−XXX

In this system, the RPO unit comprises a quartz heating assembly, a nondispersive infrared (NDIR) CO_2 detector, and a gas flow control manifold (Figures 1 and S1). The heating assembly includes (i) a programmable temperature furnace for controlled pyrolysis of OC and (ii) an isothermal oxidation furnace packed with the MnO_2 catalyst to promote quantitative conversion of the evolved carbonaceous species to CO_2. Thermal conversion follows a three-stage, oxygen-sparing workflow: (1) system purge, (2) oxygen pyrolysis/oxidation, and (3) CO_2 calibration. Samples are loaded into a quartz tube, and the system is sealed and then purged with high-purity carrier gas at 158 cc/min for 2 min. Subsequently, an Ar stream (7, 12, 22, 32, or 42 cc/min) and an Ar/O_2 mixture (8 cc/min; 5% O_2) were introduced under mass flow control, corresponding to total carrier gas flow settings of 15, 20, 30, 40, and 50 cc/min. These total carrier gas flow settings were used to optimize the CO_2 abundance reaching the CRDS cavity and thereby improve the precision of continuous $\delta^{13}C$ measurements. The programmable furnace is ramped from room temperature to 870 °C at 5 °C/min, while the evolved carbonaceous gases pass through the MnO_2 oxidation furnace where they are converted to CO_2. The CO_2 concentration is quantified by NDIR, and the detector response is calibrated using an internal standard (Ar/CH_4). To minimize the influence of instrument thermal stability on the sample−CO_2 peak profile and match $\delta^{13}C$ trends on the same temporal scale, we applied a uniform, standardized smoothing (300 points, centered running mean) procedure to the CO_2 signal to report the 300 s average value of $\delta^{13}C_{raw}$ measurements (1 Hz acquisition frequency) in this RPO-CRDS workflow, and the smoothed data were for comparative purposes only and were not included in the $\delta^{13}C$ calculations. The total analysis time of one sample for a complete temperature program is about 156 min.

The $\delta^{13}C$ value of the RPO gas was determined using CRDS,[31] and an engineered time−temperature control module was employed to ensure high measurement stability and repeatability.[35] In brief, the CO_2 product stream was continuously introduced at an inlet flow rate of 25 cc/min into a 35 cm^3 high-reflectivity cavity, with the cavity temperature and pressure maintained at ∼318.15 K and 18.7 kPa, respectively, by the internal controls.[36−39] The abundances of $^{12}C-CO_2$ and $^{13}C-CO_2$ were then measured independently by the spectroscopic ring-down time constants, and $\delta^{13}C$ was calculated using eq 1

$$\delta^{13}C\ (‰) = [(^{13}C/^{12}C)_{sample}/(^{13}C/^{12}C)_{VPDB} - 1] \times 1000 \quad (1)$$

Sample Preparation

Sample pretreatment for EC/OC was performed following previously published protocols for marine sediments.[21] Samples were weighed and transferred to 50 mL Teflon tubes precleaned with dichloromethane. Each sample was diluted with 200 mL of Milli-Q water and vacuum-filtered through a 47 mm quartz fiber filter. The filters were freeze-dried (12 h), then sealed, and stored refrigerated until analysis. To ensure accurate sediment measurements using the EC/OC approach, we evaluated and confirmed the effect of sample mass on analytical results. The marine sediment was loaded onto quartz filters at five masses (pretreatment ∼0.03 to 0.50 g at 40 mm × 40 mm). Each quartz filter can be sectioned into 4−5 replicates with a fixed area (10 mm × 15 mm) to promote spatial homogeneity and ensure reliable carbon determination.

Acidification is a key step to remove inorganic carbon (IC) from sediments before determining $\delta^{13}C$-OC. We used an HCl-rinsing procedure following established protocols.[20,21,40] Sediment samples were freeze-dried, homogenized, and placed in Teflon tubes. Aliquots of 1 N HCl (5 mL per addition, total 10 mL) were added repeatedly at room temperature. The samples were then heated in a water bath at 60 °C for 1 h. Residues were separated from the supernatant by centrifugation (2500 rpm, 2 min) and rinsed with Milli-Q water. To minimize the losses of carbonaceous material, the number of rinses was kept as low as possible, while ensuring that the sample was acid-free.[41] Acid treatment removes carbonates and can also extract some metals (e.g., Fe, Cu),[42] thereby limiting the oxygen supplied by metal oxides and helping to minimize the hydrolysis of organic matter. After acidification, the residue typically appeared brown; samples were then lyophilized, transferred to Petri dishes, sealed with aluminum foil, and stored cold until analysis. In addition, the international standards were directly applied to precombusted quartz filters without acidification.

QA/QC, Calibration, and Data Processing

Before each analytical batch, procedural and instrument blanks were analyzed, and the limit of detection (LOD)/quantitation was calculated from blank variability. CO_2-abundance thresholds were enforced when reporting $\delta^{13}C$ to maintain precision.

Blanks and Detection Limits

Blank CO_2 was characterized using a blank quartz filter without sediment under the same temperature program and carrier gas composition as the sediment analyses (Ar 7 cc/min and Ar/O_2 8 cc/min). Blank background levels were quantified from the raw $^{12}CO_2$ and raw $^{13}CO_2$ signals during the first 8000 s of the run, prior to the CH_4 calibration pulse. Under these conditions, the RPO-CRDS system yielded stable blank levels below 2 ppm, with mean values of $^{12}CO_2$ = 1.280 ppm and $^{13}CO_2$ = 0.016 ppm in the first run (Figures 2 and S2). All blank calculations were based on the raw CO_2 signals rather than the smoothed curves. One blank run was performed before each analytical batch, and additional blank checks were carried out whenever a new Ar or Ar/O_2 gas cylinder was introduced. In routine operation, one blank run was sufficient before each batch of sediment analyses. Repeated blank tests showed that the first two nearly consecutive blanks remained stable, whereas later consecutive blanks exhibited pronounced

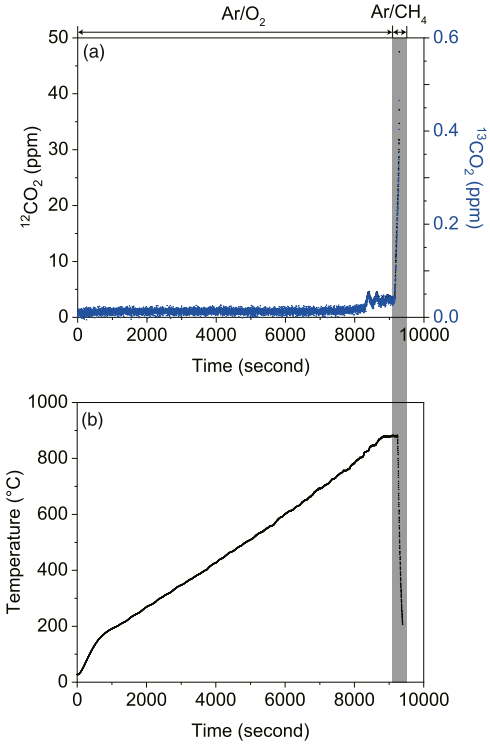


Figure 2. Time alignment and blank characterization of the sequential RPO-CRDS run. (a) Continuous CRDS traces of $^{12}CO_2$ (black, left axis) and $^{13}CO_2$ (blue, right axis) during a full temperature program under the Ar/O_2 carrier. The baseline remains near the instrumental blank throughout most of the run; the shaded interval marks the brief Ar/CH_4 pulse injected at the end of the program as an internal standard for precise time alignment between the RPO and CRDS data streams. (b) Corresponding furnace temperature ramp $T(t)$: rapid warm-up to ∼150 °C, followed by a linear increase to ∼870 °C, and a short hold over the same time domain as (a). The CH_4 pulse observed in (a) is used to compute the transport delay Δt and to register CRDS time stamps to the RPO time−temperature map for constructing T-CO_2 and T-$\delta^{13}C$ profiles.

https://doi.org/10.1021/acs.analchem.6c00100
Anal. Chem. XXXX, XXX, XXX−XXX

variability (Figure S2) due to incomplete thermal re-equilibration of the heated system. Therefore, additional blank or sediment runs were performed only after the system had returned to a stable state, which, in our setup, typically required more than 24 h.

To set CO_2-abundance thresholds quantitatively, we used a first-order error-propagation model for CRDS isotope ratios.[38,43] For the simultaneous measurement of $^{13}CO_2$ and $^{12}CO_2$, the short-term $\delta^{13}C$ precision (σ_δ, ‰, rms) scales with the inverse square root of the inlet CO_2 abundance C (ppm) and the averaging time τ (s) dependence from shot-noise or white-noise statistics according to eq 2[39,44]

$$\sigma_\delta(C, \tau) \approx \frac{K}{\sqrt{C}} \frac{1}{\sqrt{\tau}} \tag{2}$$

where K is an instrument-specific constant that lumps absorption signal-to-noise ratio (SNR) and optical noise. The magnitude of the empirical constant K can be corroborated by back calculation from manufacturer specifications and published performance at different averaging times. Using a representative CRDS specification of $\delta^{13}C \approx 0.25$‰ at 200 ppm (5 min) as an example, $K \approx 60$.[39,44] The corresponding 1 s value is $K \approx 3$, assuming white-noise scaling with averaging time. Thus, the minimum CO_2 abundance required to achieve a target precision σ_δ^* according to eq 3

$$C_{req}\ (\text{ppm}) \approx \left(\frac{K}{\sigma_\delta^*}\right)^2 \frac{1}{\tau} \tag{3}$$

Practical thresholds derived from this expression (for $\tau = 1$ or $\tau = 300$) are as follows.

For 1 s reporting, $\delta^{13}C_{raw}$ denotes the raw CRDS-reported $\delta^{13}C$ values prior to temporal averaging. Under these conditions ($\tau = 1$ s; $K \approx 3$), the estimated CO_2 abundance required to achieve target precisions of 0.5, 0.3, 0.2, and 0.15‰ is approximately 40, 100, 225, and 400 ppm, respectively.

For 300 s averaging, $\delta^{13}C_{5\ min}$ denotes the temporally averaged value; under these conditions ($\tau = 300$ s; $K \approx 60$), the corresponding abundance thresholds are approximately 50, 130, 300, and 550 ppm, respectively.

Because 1 s CRDS output is used to construct the continuous thermogram, we selected $C \geq 100$ ppm as the practical threshold for quantitative $\delta^{13}C$ reporting, corresponding to an expected precision of 0.3‰.[39,45] In addition, we also report the precision of 0.5‰ ($C \geq 40$ ppm) for presentation and comparison; this is only qualitative context but excluded from quantitative interpretation.

Correction for $\delta^{13}C$ Values

Rationale: Because $\delta^{13}C$ is defined by the isotope ratio $R = {}^{13}C/{}^{12}C$ relative to the Vienna Pee Dee Belemnite (VPDB), blank removal cannot be performed by simple subtraction. Therefore, we correct in ratio space using a two-endmember mixing model and then convert back to $\delta^{13}C$, for removing contributions from residual CO_2 in the flow path and analyzer background. C denotes the CO_2 abundance (ppm) and δ denotes the VPDB-referenced $\delta^{13}C$ (‰). Subscripts tot, b, and s refer to the total (sample + blank), blank (no sample), and blank-corrected sample, respectively. R_{VPDB} is the VPDB reference ratio.

(1) Measure blanks under controlling T/P: record C_b and δ_b.
(2) Acquire sample: for each time point, record C_{tot} and δ_{tot}.
(3) Convert δ to ratios according to eqs 4 and 5

$$R_{tot} = R_{VPDB}\left(1 + \frac{\delta_{tot}}{1000}\right) \tag{4}$$

$$R_b = R_{VPDB}\left(1 + \frac{\delta_b}{1000}\right) \tag{5}$$

(4) Blank removal in ratio space according to eq 6

$$R_s = \frac{R_{tot}C_{tot} - R_bC_b}{C_{tot} - C_b} \tag{6}$$

(5) Convert back to δ according to eq 7

$$\delta_s = 1000\left(\frac{R_s}{R_{VPDB}} - 1\right) \tag{7}$$

Assign Pyrolysis Temperature to the CRDS Inlet Gas

The RPO unit outputs a 1 Hz time series containing furnace temperature $T(t)$ and the internal-standard pulse (CH_4), covering the entire 156 min (Figures 2 and S1). The CRDS unit records its own time together with $^{12}CO_2$ and $^{13}CO_2$ signals. To assign a pyrolysis temperature to each CRDS data point, we first align the two instruments in time by matching the CH_4 internal standard peak observed in both datasets (Figures 1 and S1). The peak alignment yields a transport delay Δt from the RPO outlet to the CRDS inlet; the CRDS time axis is then shifted by $-\Delta t$. After alignment, the RPO time–temperature map $T(t)$ is applied to the CRDS stream (Figures 2 and S1) to obtain temperature-resolved arrays, i.e., T-$^{12}CO_2$ and T-$^{13}CO_2$ (and subsequently T-$\delta^{13}C$).

Practically, both series are resampled to a common grid, and quality control checks (single sharp CH_4 peak, consistent Δt) are enforced. We provide a companion framework and code that performs (i) CH_4 peak detection, (ii) time lag estimation, (iii) resampling to a common grid, and (iv) construction of T-$^{12}CO_2$ and T-$^{13}CO_2$ data products. The $\delta^{13}C$ was calculated separately because it requires independent determination by laboratory-specific background values. The code is provided in the Supporting Information.

$\delta^{13}C$ Calibration by International Standard Samples

Matrix consideration: Because the CRDS analyzer is factory-optimized for air matrices, operation under the carrier gas (Ar 7 cm^3/min and Ar/O_2 8 cm^3/min) introduces a matrix mismatch that shifts the raw displayed $\delta^{13}C$ values relative to the VPDB scale. We therefore recalibrated the system under the actual carrier gas conditions using three international reference materials (IA-R006, IAEA-600, and USGS-64) spanning the sample range.[38,43,45]

Standards: We analyzed bulk international standards spanning from −11.64 to −40.81‰ (IA-R006, −11.64‰, 42.1 wt %; IAEA-600, −27.77‰, 49.5 wt %; USGS-64, −40.81‰, 32.0 wt %),[46,47] employing the gas storage coil method,[29] to anchor the calibration across the sample range (Figures 3 and S3 and Table 1).

Abundance threshold and integration: Following the CO_2-abundance requirement in in Section Instrumentation, we integrated $^{12}CO_2$ and $^{13}CO_2$ only within temperature windows where the inlet CO_2 met $C \geq 100$ ppm, and we also removed the blank values ($^{12}CO_2$ = 1.28 ppm and $^{13}CO_2$ = 0.016 ppm, more details in Section Blanks and Detection Limits). These integrations yield bulk-equivalent $\delta^{13}C$ values for each standard at multiple carbon loads. Here, uncorrected $\delta^{13}C$ refers to the raw CRDS-reported values prior to standard-based calibration, whereas corrected $\delta^{13}C$ refers to the values after application of the empirical calibration equation. Separately, the CO_2 threshold of 100 ppm is far below the international standard CO_2 peak (Figure S3) and was used to define abundance-compliant intervals for quantitative reporting. A linear regression derived from the standards was used to correct all measurements according to eq 8

$$\delta^{13}C_{corrected} = a \times \delta^{13}C_{uncorrected} + b \tag{8}$$

where a and b are the slope and intercept obtained from standards analyzed at varying carbon contents (20–100 μg of C), $a = 1.06978$ and $b = 50.28657$. The corrected $\delta^{13}C$ shows agreement with the international standard values across sample sizes (Figure 3 and Table 1), with residuals typically within −0.70 to 0.85‰ under abundance-compliant conditions. Theoretically, the factory-specified precision of the CRDS analyzer for $\delta^{13}C$ measurements is <0.1‰ (1-σ, over a 1 h interval with 5 min averaging). This −0.70 to 0.85‰ error reflects the nonlinear discrepancy between the reflectance spectra of Ar/O_2 carrier gas and air.[29] Scale normalization to the VPDB used three reference materials spanning the sample range of complex OC.[46]

https://doi.org/10.1021/acs.analchem.6c00100
Anal. Chem. XXXX, XXX, XXX−XXX

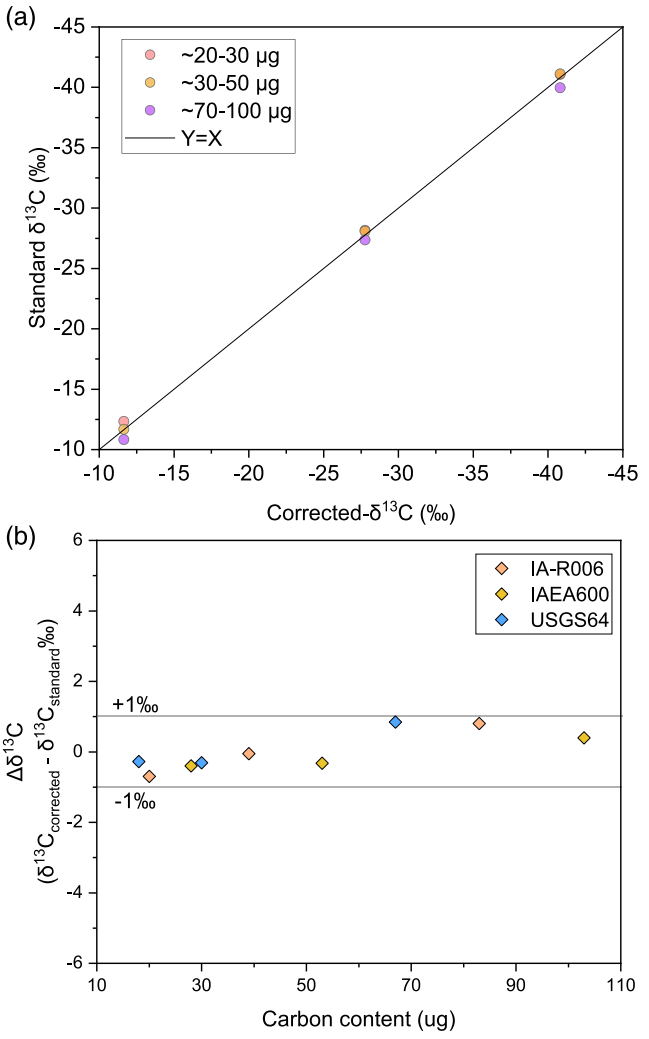


Figure 3. Comparison of $\delta^{13}C$ between standards and CRDS measurements based on the Ar/O_2 gas flow. (a) Scatter shows certified standard $\delta^{13}C$ (y-axis) versus corrected $\delta^{13}C$ (x-axis) for multiple carbon loads (symbol size: 20−100 μg). (b) Calibration points span the sample range (−11.64 to −40.81‰), and residuals after correction are ≤1‰ (see Table 1).

Table 1. $\delta^{13}C$ Calibrations with International Reference Materials

isotope standard sample	weight mass/carbon content (μg)	standard $\delta^{13}C$ (‰)	corrected-$\delta^{13}C$ (‰)
IA-R006	48 (20)	−11.64	−12.34
	93 (39)		−11.69
	198 (83)		−10.83
IAEA-600	58 (28)	−27.77	−28.17
	108 (53)		−28.09
	209 (103)		−27.37
USGS-64	57 (18)	−40.81	−41.08
	95 (30)		−41.12
	209 (67)		−39.96

RESULTS AND DISCUSSION

Optimization of the Carrier Gas Flow and Sample Mass Selection for Natural Sediments

The combination of inlet gas flow and sample mass sets the instantaneous CO_2 abundance seen by the CRDS, which further influences the reported windows ($CO_2 \geq 100$ ppm) in the RPO-CRDS system defined in Section QA/QC, Calibration, and Data Processing. In addition, to minimize grain size-related heterogeneity among aliquots between runs, the marine samples were pretreated and wet-sieved to <20 μm. In the following, we use a representative marine sediment (ME03 < 20 μm, TOC%: 0.99 ± 0.03%)[21] to illustrate the influence of the carrier gas flow and sample mass in the RPO-CRDS system.

Effect of the Carrier Gas Flow on CO_2 Abundance and $\delta^{13}C$ Precision

Carrier gas flow is a primary control on the accuracy of the temperature-$\delta^{13}C$ profile, as a higher flow rate dilutes the entered CO_2 abundance at the CRDS inlet. At a fixed sediment mass, changing the Ar flow (while keeping the Ar/O_2 composition constant at 8 cc/min) directly modulates the peak CO_2 (ppm) and thus $\delta^{13}C$ precision. We tested five various total carrier gas flows (15, 20, 30, 40, 50 cc/min) on the same sediment (Figures 4 and S4).

As expected, lower flow corresponded to higher CO_2 (ppm) in CRDS analysis because the evolved carbon per unit time is partitioned into a smaller carrier gas volume. This low-flow regime stabilizes $\delta^{13}C$ by improving the signal-to-noise ratio in the abundance-compliant windows (Section QA/QC, Calibration, and Data Processing). In our system, the CRDS pump imposes a practical lower bound; 15 cc/min delivered the highest inlet CO_2 among the tested conditions and falls within the sample flow (<50 standard cubic centimeters per minute) and pressure operating window (300−1000 Torr) of the CRDS analyzer used here.

Sample Mass, Carbon Yield, and Abundance-Compliant Temperature Windows

At a fixed inlet flow, the sample mass scales the inlet peak value of CO_2 nearly proportionally (Figures 4b and S5). For the tested loads (pretreatment 0.03−0.50 g sediments), higher mass increased the fraction of the temperature program that satisfied the abundance threshold and reduced pointwise scatter in $\delta^{13}C$ values. Consistent with Section QA/QC, Calibration, and Data Processing, we recommend selecting a mass flow pair that yields $C \geq 100$ ppm across the thermal domain of interest and exerts a first-order control on $\delta^{13}C$ precision (Figure 4 and Section QA/QC, Calibration, and Data Processing); in practice, ∼0.2 to 0.5 g at 15 cc/min is sufficient for most marine sediments in our matrix, while lower carbon or highly refractory samples may require larger mass. Under 15 cc/min, the $C \geq 100$ ppm window typically spans from ∼250 to 600 °C, covering ∼92.4% of the integrated CO_2 release for the test sediment, with $\delta^{13}C$ values ranging from −19.38 to −25.12‰ (Figures 4, S4, and S5).

Hence, we suggest the following: (i) start at 15 cc/min carrier gas (Ar and Ar/O_2) with ∼0.20 to 0.50 g sediment; (ii) verify that the target temperature window (e.g., 250−600 °C) meets $C \geq 100$ ppm; if not, increase mass; and (iii) report the continuous $\delta^{13}C$ curve only within abundance-compliant intervals.

Reproducibility Assessment for Natural Sediments

To evaluate the precision and repeatability of $\delta^{13}C$ curves measured by the RPO-CRDS system, the natural marine sediment (ME03 < 20 μm; ∼0.5 g total load per filter) has been analyzed four times in succession (Figures 5 and S6). The results show excellent reproducibility for both the CO_2 evolution and the continuous $\delta^{13}C$ profile. As shown in Figures 5a and S6, the minor differences among CO_2 and $\delta^{13}C$ curves are primarily reflected by small variations in the loaded sediment

https://doi.org/10.1021/acs.analchem.6c00100
Anal. Chem. XXXX, XXX, XXX−XXX

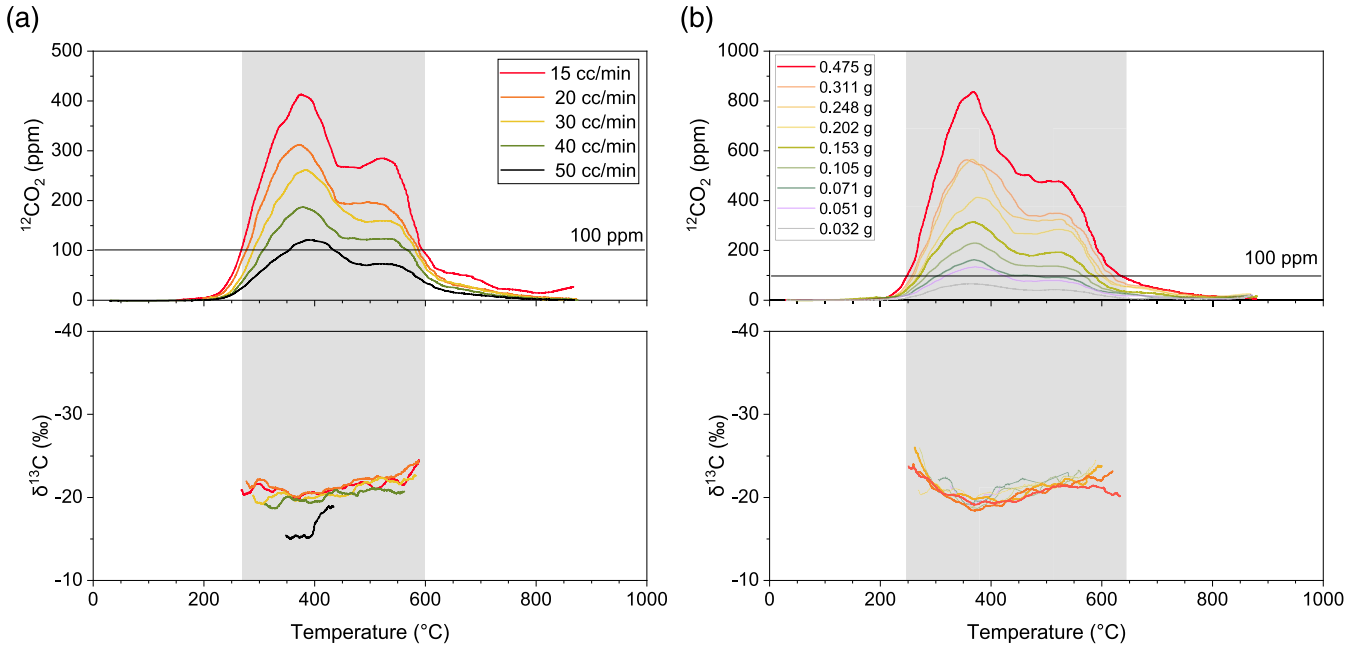


Figure 4. Effect of the carrier gas flow or CO_2 abundance and the continuous $\delta^{13}C$ curve. Fixed sediment mass and Ar/O_2 composition held constant. (a) $^{12}CO_2$ concentration versus temperature at five total flows at 0.202 g sediments (legend: 15, 20, 30, 40, 50 cc/min). (b) $^{12}CO_2$ concentration versus temperature for nine loadings (0.032−0.475 g; color legend). The horizontal line marks 100 ppm, and the gray band (~250 to 600 °C) highlights the abundance-compliant window used for quantitative $\delta^{13}C$ reporting.

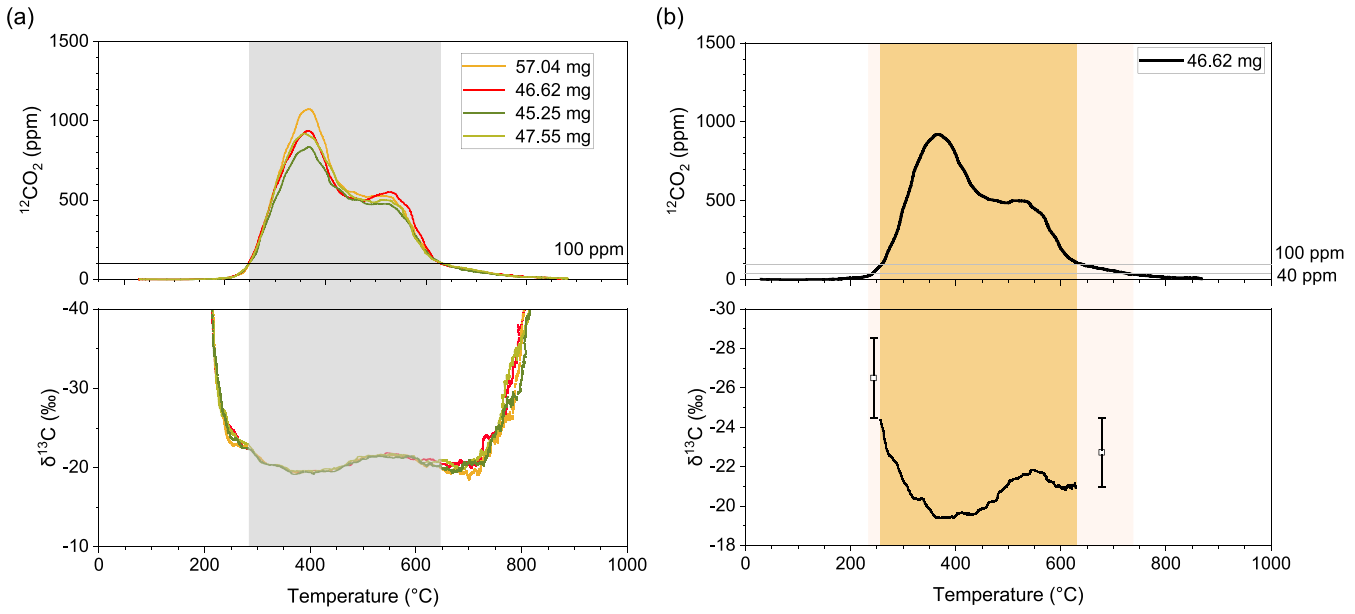


Figure 5. Reproducibility and example application to a natural sediment (ME03 < 20 μm). (a) Temperature-$^{12}CO_2$ traces from four replicate aliquots (46.62−57.04 mg) analyzed under identical carrier gas conditions (Ar/O_2 8 cc/min and Ar 7 cc/min). The horizontal line marks 100 ppm, and the gray band (~250 to 600 °C) denotes the abundance-compliant window used for quantitative $\delta^{13}C$ reporting. CO_2 evolution curves overlap closely, with minor amplitude differences attributable to small mass variations. (b) Temperature-$\delta^{13}C$ trace for an ME03 < 20 μm aliquot (46.62 mg) under Ar/O_2 8 cc/min + Ar 7 cc/min. Horizontal lines mark 40 and 100 ppm inlet CO_2. Shaded bands indicate temperature intervals where the theoretical CRDS precision is 0.3‰ (orange, CO_2 > 100 ppm) and 0.5‰ (light orange, CO_2 > 40 ppm) at the chosen averaging time. Error bar symbols illustrate representative averages within (right) and near the edge of (left) the compliant windows; segments outside the orange-shaded intervals are retained for qualitative context but excluded from quantitative interpretation.

mass: ~0.5 g of sediment was distributed over a 47 mm quartz filter, from which 10 mm × 15 mm rectangular coupons were cut for each running time, inevitably leading to a slight mass variability.[48] The standard deviation (SD) of $\delta^{13}C$ across the four curves was ≤0.5‰. These statistics confirmed that the method delivers high precision and robustness for complex organic matter.

In addition, the abundance-compliant interval of the marine sediment (ME03 < 20 μm) was further integrated to derive a bulk-equivalent $\delta^{13}C$ estimate. Across replicate aliquots (~0.5 g total load per filter, 15 cc/min total carrier gas flow, acid rinsing),

https://doi.org/10.1021/acs.analchem.6c00100
Anal. Chem. XXXX, XXX, XXX−XXX

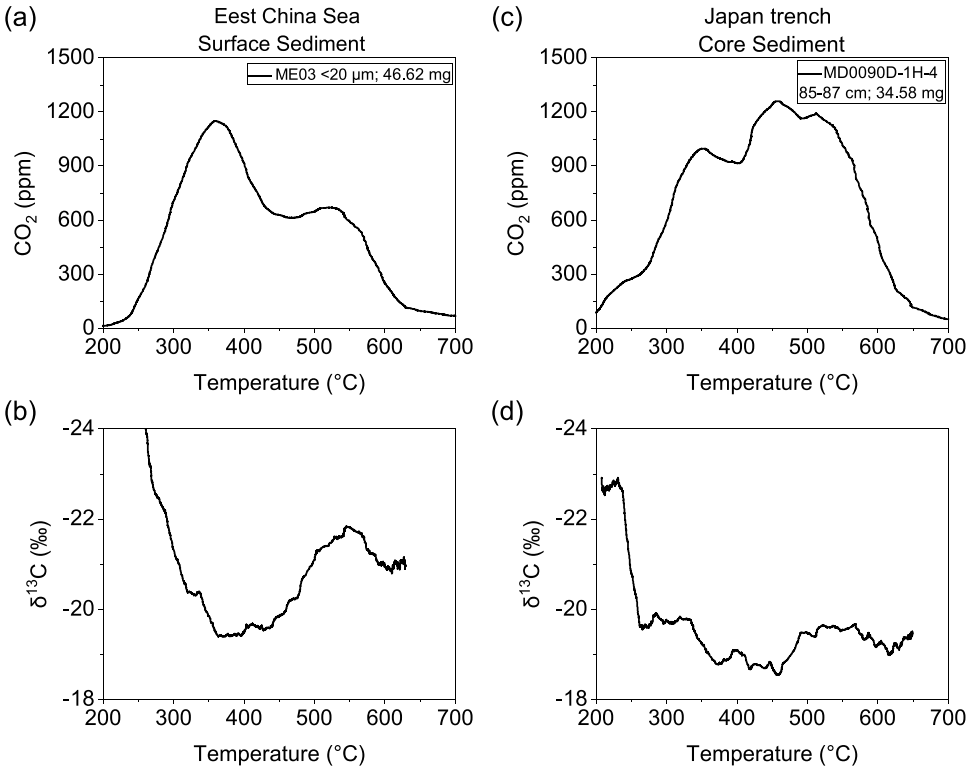


Figure 6. Comparison of temperature-resolved CO_2 release and $\delta^{13}C$ profiles for the East China Sea surface sediment and Japan Trench core sediment. (a, b) East China Sea surface sediment (ME03 < 20 μm; 122.58°E, 28.73°N; water depth: 63 m).[21] (c, d) Japan Trench core sediment (IODP386, MD0090D-1H-4, 85−87 cm; 144.06°E, 38.30°N; water depth: 7450 m).[50] (a, c) CO_2 release versus temperature and (b, d) corresponding continuous $\delta^{13}C$ profiles reported only where CO_2 > 100 ppm. The two sediments display distinct CO_2 thermograms and $\delta^{13}C(T)$ trajectories, indicating different distributions of isotopically distinct carbon across thermal stability domains.

the resulting RPO-CRDS bulk-equivalent values ranged from −20.35 to −20.60‰, which are slightly higher than the previously reported bulk $\delta^{13}C$ value (acid fumigation) of −21.4‰ for the same sedimentary material.[49] This offset most likely reflects the exclusion of low-abundance carbon (<100 ppm) released outside the abundance-compliant interval (Figures 5a and S7), together with different thermal temperatures and acid treatments for bulk $\delta^{13}C$ measurements between acid rinsing and fumigation.[20]

Application of the RPO-CRDS System in Marine Sediments

As shown in Figure 5, the continuous $\delta^{13}C(T)$ profile can be subdivided into three broad domains with relatively different reactivities—a labile fraction (∼250 to 400 °C), a resistant fraction (∼400 to 550 °C), and a refractory fraction (∼550 to 650 °C), each characterized by distinct $\delta^{13}C$ traces. This pattern indicates that sedimentary OC acts as a potential superposition of pools differing in thermal stability. Importantly, the $\delta^{13}C$ shifts are asynchronous with carbon release (Figure 5b), suggesting that the observed profiles reflect the combined effects of source heterogeneity, molecular composition, mineral protection, and microbial remodeling,[25,50−54] rather than source differences alone.[48,55,56]

More specifically, the labile fraction (250−400 °C) releases lower activation energy biopolymers (polysaccharides, proteins) with lipids; lipid ^{13}C-depletion accounts for the more negative $\delta^{13}C$, and shallow-burial secondary production/priming can modulate this window's contribution and instantaneous isotopic expression.[57−59] The slow fraction (400−550 °C) isolates higher activation energy, cross-linked/condensed macromolecules (e.g., lignin-derived aromatics, algaenan residues), and mineral-associated OM; microbial carbon is preferentially retained on minerals, yielding $\delta^{13}C$ between marine (−19 to −22‰) and C_3 terrestrial (−27 to −30‰) endmembers.[7,57,58,60,61] The refractory fraction (550−650 °C) is dominated by highly condensed aromatic carbon or graphite carbon,[62] with a $\delta^{13}C$ of ∼−28 to −21‰, consistent with high-impact constraints on marine refractory DOC or long-term selective preservation of microbial refractory carbon.[58,63]

From an OC cycling perspective, the $\delta^{13}C(T)$ framework allows us to distinguish between genuinely uniform subreservoirs and apparent homogeneity that arises only from averaging. For example, sections of the temperature-$\delta^{13}C$ curve that exhibit smooth, monotonic trends likely reflect relatively coherent stability units, whereas inflections, plateaus, or reversals indicate mixtures of subreservoirs with different origins or degradation histories. Hence, continuous RPO-CRDS spectra therefore provide more than higher data density: they reveal where in stability space different OC subreservoirs are concentrated, where they interact or exchange carbon and isotopes, and which parts of the reservoir are most sensitive to environmental or diagenetic perturbations.

To evaluate the applicability of this framework to natural sediments, we applied the RPO-CRDS system to two natural marine sediments from contrasting depositional environments: an East China Sea surface sediment (ME03; 122.58°E, 28.73°N; water depth: 63 m)[21] and a Japan Trench core sediment (IODP386, MD0090D; 144.06°E, 38.30°N; water depth: 7450 m).[50] Analyses were performed on 0.5 g of dried sediment with a total carrier at 15 cc/min. The sample was stored at −20 °C from collection to analysis to minimize microbial alteration and

https://doi.org/10.1021/acs.analchem.6c00100
Anal. Chem. XXXX, XXX, XXX−XXX

preserve the native OC isotopic signal. This comparison was designed to test whether the method can resolve not only isotopic heterogeneity within a single sediment[48,64] but also the differences in the organization of carbon pools between marginal sea and trench depositional environments. As shown in Figure 6, both two sediments show heterogeneity with the continuous temperature-resolved CO_2 and $\delta^{13}C$ profiles in different depositional environments. The East China Sea surface sediment shows a CO_2 thermogram with a dominant peak centered in the lower temperature domain (~330 to 390 °C) and a secondary shoulder in the intermediate- to higher temperature domain (~470 to 560 °C). In contrast, the Japan Trench core sediment exhibits a broader CO_2 release structure, with substantial carbon release extending across the intermediate- and high-temperature interval (~320 to 580 °C) and a stronger high-temperature contribution overall. This difference indicates that the trench core contains a larger proportion of thermally stable organic carbon relative to the marginal-sea surface sediment.

The two depositional environment sediments also differ clearly in their $\delta^{13}C(T)$ trajectories. In the East China Sea sample, $\delta^{13}C$ varies strongly with temperature, becoming less negative through the main intermediate-temperature interval and then shifting again toward more negative values in the refractory domain. By contrast, the Japan Trench core displays a narrower and generally heavier $\delta^{13}C$ pattern across most of the abundance-compliant interval, after an initial low-temperature excursion. On the other hand, the East China Sea sediment expresses stronger isotopic separation among low-, intermediate-, and high-temperature carbon pools, whereas the Japan Trench sediment shows a more compressed isotopic range concentrated in thermally more stable domains. These contrasts are more consistent with differences in how OC is partitioned among labile, resistant, and refractory fractions in the two settings. For the East China Sea surface sediment, the stronger low-temperature contribution and larger isotopic contrast may reflect a more heterogeneous mixture including relatively fresh, lipid-rich, and weakly protected organic matter together with isotopically distinct refractory components.[65−67] For the Japan Trench core sediment, the broader high-temperature CO_2 release pattern and relatively heavier main $\delta^{13}C$ domain may reflect a greater contribution from thermally stable, more extensively reworked, selectively preserved, or mineral-associated organic carbon during downslope transport, burial, and postdepositional alteration.[25,50,51] These interpretations remain first-order, but they show that continuous RPO-CRDS thermograms can distinguish not only within-sample isotopic heterogeneity but also between-sample redistribution of carbon across stability space.

Overall, the primary advantage of the RPO-CRDS system lies in its data acquisition paradigm, which performs >5000 measurements during a standard run. The RPO-CRDS system provides a continuous, high-resolution $\delta^{13}C$ profile for capturing small carbon but isotopic shift, revealing the potential tipping point of source changes in stability. This allows researchers to explore how much carbon is stored in different stability units, which source domains control carbon flux and isotopes, and which parts of the reservoir respond most strongly to environmental change in marine sediments. In addition, this method can be applicable to investigating the dynamics of soils, aerosols, and other low-carbon materials. The ability to obtain a continuous $\delta^{13}C$ thermogram provides a new dimension of data that can be integrated with other analysis techniques for a more holistic mixture OC understanding of carbon cycling across Earth's systems.

CONCLUSIONS

We developed an online RPO-CRDS system that converts a single 156 min CO_2 gas run into a continuous, high-resolution temperature-$\delta^{13}C$ profile. In this framework, the sediment OC is no longer represented by a bulk value but is viewed as a continuous distribution in degradability for its sources to reveal internal dynamic behavior. In addition, we established an abundance-based precision model, practical CO_2 thresholds, and system blank and $\delta^{13}C$ calibration by international reference materials (IA-R006, IAEA-600, USGS-64). Hence, the RPO-CRDS system provides both a new view of sedimentary OC and an analytical tool that can be applied to both sediments, soils, aerosols, and other low-carbon materials to link $\delta^{13}C$ measurements to mechanistic models of carbon stabilization and source contributions.

ASSOCIATED CONTENT

Supporting Information

The Supporting Information is available free of charge at https://pubs.acs.org/doi/10.1021/acs.analchem.6c00100.

Code for time alignment and construction of temperature-resolved CO_2 and $\delta^{13}C$ data products (Figures S1−S7) (PDF)

AUTHOR INFORMATION

Corresponding Author

Rui Bao − *Frontiers Science Center for Deep Ocean Multispheres and Earth System, Key Laboratory of Marine Chemistry Theory and Technology, Ministry of Education/Institute for Advanced Ocean Studies, Ocean University of China, Qingdao 266100, China; Laboratory for Marine Geology, Qingdao Marine Science and Technology Center, Qingdao 266237, China*; Email: baorui@ouc.edu.cn

Authors

Yipeng Wang − *Frontiers Science Center for Deep Ocean Multispheres and Earth System, Key Laboratory of Marine Chemistry Theory and Technology, Ministry of Education/Institute for Advanced Ocean Studies, Ocean University of China, Qingdao 266100, China; Laboratory for Marine Geology, Qingdao Marine Science and Technology Center, Qingdao 266237, China*; orcid.org/0009-0005-3997-0287

Mingzhi Liu − *Frontiers Science Center for Deep Ocean Multispheres and Earth System, Key Laboratory of Marine Chemistry Theory and Technology, Ministry of Education/Institute for Advanced Ocean Studies, Ocean University of China, Qingdao 266100, China; Laboratory for Marine Geology, Qingdao Marine Science and Technology Center, Qingdao 266237, China*

Yupeng Cao − *Chongben Honors College, Ocean University of China, Qingdao 266100, China*

Weiran Hu − *Frontiers Science Center for Deep Ocean Multispheres and Earth System, Key Laboratory of Marine Chemistry Theory and Technology, Ministry of Education/Institute for Advanced Ocean Studies, Ocean University of China, Qingdao 266100, China; Laboratory for Marine*

https://doi.org/10.1021/acs.analchem.6c00100
Anal. Chem. XXXX, XXX, XXX−XXX

Geology, Qingdao Marine Science and Technology Center, Qingdao 266237, China

Yekai Wang − *Frontiers Science Center for Deep Ocean Multispheres and Earth System, Key Lab of Submarine Geosciences and Prospecting Techniques, Ministry of Education and College of Marine Geosciences, Ocean University of China, Qingdao 266100, China*

Nan Wang − *Frontiers Science Center for Deep Ocean Multispheres and Earth System, Key Lab of Submarine Geosciences and Prospecting Techniques, Ministry of Education and College of Marine Geosciences, Ocean University of China, Qingdao 266100, China*

Longhai Zhu − *College of Marine Geo-Science and Key Lab of Submarine Geosciences and Prospecting Techniques, Ministry of Education, Ocean University of China, Qingdao 266100, China*

Complete contact information is available at: https://pubs.acs.org/10.1021/acs.analchem.6c00100

Author Contributions

Conceptualization: Yipeng W. and R.B. Methodology: Yipeng W., R.B., N.W., M.L., and L.Z. Investigation: Yipeng W., R.B., M.L., W.H., Yekai W., and Y.C. Visualization: Yipeng W., R.B., and W.H. Funding acquisition: R.B. and Yipeng W. Project administration: R.B.

Notes

The authors declare no competing financial interest.

■ ACKNOWLEDGMENTS

This study was supported by the National Natural Science Foundation of China (42525604, R.B.), National Natural Science Foundation of China (424B2047, Y.W.), National Key R&D Program of China (2025YFF0516900 & 2025YFF0516903, R.B.), National Natural Science Foundation of China (42525604, R.B.). We thank Dr. Bruce Weng, Peng Fu, and Huiqiang Li for guidance on software modification and the engineering team for technical support. We are grateful to the *Dongfanghong II* ship crew and the IODP community for assistance with natural sample collection, and the two anonymous reviewers for their constructive comments.

■ ABBREVIATIONS

CRDS, cavity ring-down spectroscopy; CSIA, compound-specific isotope analysis; IAEA, International Atomic Energy Agency; IC, inorganic carbon; IRMS, isotope ratio mass spectrometry; LOD, limit of detection; LOQ, limit of quantitation; NDIR, nondispersive infrared; OC, organic carbon; OC%, organic carbon content; wt %, weight percent concentration; OCEC, organic carbon-elemental carbon analyzer; OM, organic matter; QA/QC, quality assurance/quality control; RPO, ramped pyrolysis/oxidation; RSD, relative standard deviation; SD, standard deviation; SNR, signal-to-noise ratio; USGS, United States Geological Survey; VPDB, Vienna Pee Dee Belemnite; $\delta^{13}C$, stable carbon isotope, ratio of $^{13}C/^{12}C$ relative to VPDB

■ REFERENCES

(1) Berner, R. A. Atmospheric Carbon Dioxide Levels Over Phanerozoic Time. *Science* **1990**, *249*, 1382−1386.

(2) Blattmann, T. M.; Liu, Z.; Zhang, Y.; Zhao, Y.; Haghipour, N.; Montluçon, D. B.; Plötze, M.; McIntyre, C.; Haghipour, S.; Eglinton, T. I. Mineralogical control on the fate of continentally derived organic matter in the ocean. *Science* **2019**, *366*, 742−745.

(3) Berner, R. A.; Caldeira, K. The need for mass balance and feedback in the geochemical carbon cycle. *Geology* **1997**, *25*, 955−956.

(4) Zhang, Y.-L.; Kawamura, K.; Agrios, K.; Lee, M.; Salazar, G.; Szidat, S. Fossil and Nonfossil Sources of Organic and Elemental Carbon Aerosols in the Outflow from Northeast China. *Environ. Sci. Technol.* **2016**, *50*, 6284−6292.

(5) Yi, Y.; Tanentzap, A. J.; He, C.; Merder, J.; Osterholz, H.; Bao, H.; Hawkes, J. A.; Cai, R.; Li, S.-L.; Shi, Q.; Xu, S.; Zhang, C.; Liu, C.-Q.; Zhao, M.; He, D. Underestimated input of terrestrial dissolved organic carbon to the ocean. *Proc. Natl. Acad. Sci. U.S.A.* **2025**, *122* (45), No. e2505838122.

(6) Hedges, J. I.; Keil, R. G. Sedimentary organic matter preservation: an assessment and speculative synthesis. *Mar. Chem.* **1995**, *49*, 81−115.

(7) Hemingway, J. D.; Hilton, R. G.; Selvaraj, K.; Adhikari, D. P.; Pearl, J. K.; Galy, V. V.; Xu, X.; Eglinton, T. I. Mineral protection regulates long-term global preservation of natural organic carbon. *Nature* **2019**, *570*, 228−231.

(8) Yang, Z.; Xing, L.; Che, Y.; Wang, N.; Ma, H.; Zhao, S.; Chen, A.; Li, H.; Bao, R. Interaction between organic carbon conversion and microbial metabolism in marginal seas sediments during hydrodynamic sorting processes. *J. Geophys. Res.: Oceans* **2025**, *130* (4), No. e2024JC021994.

(9) Hemingway, J. D.; Hilton, R. G.; Hovius, N.; Eglinton, T. I.; Haghipour, N.; Wacker, L.; Chen, M.-C.; Galy, V. V. Microbial oxidation of lithospheric organic carbon in rapidly eroding tropical mountain soils. *Science* **2018**, *360* (6385), 209−212.

(10) Bao, R.; van der Voort, T. S.; Zhao, M.; et al. Influence of Hydrodynamic Processes on the Fate of Sedimentary Organic Matter on Continental Margins. *Global Biogeochem. Cycles* **2018**, *32*, 1420−1432.

(11) Burdige, D. J. Preservation of Organic Matter in Marine Sediments: Controls, Mechanisms, and an Imbalance in Sediment Organic Carbon Budgets? *Chem. Rev.* **2007**, *107*, 467−485.

(12) Hatcher, P. G.; Spiker, E. C.; Szeverenyi, N. M.; Maciel, G. E. Selective preservation and origin of petroleum-forming aquatic kerogen. *Nature* **1983**, *305*, 498−501.

(13) Lehmann, J.; Kleber, M. The contentious nature of soil organic matter. *Nature* **2015**, *528*, 60−68.

(14) Peterson, B. J.; Fry, B. Stable Isotopes in Ecosystem Studies. *Annu. Rev. Ecol. Syst.* **1987**, *18*, 293−320.

(15) Laws, E. A.; Popp, B. N.; Bidigare, R. R.; Kennicutt, M. C.; Macko, S. A. Dependence of phytoplankton carbon isotopic composition on growth rate and $[CO_2)aq$: Theoretical considerations and experimental results. *Geochim. Cosmochim. Acta* **1995**, *59*, 1131−1138.

(16) The Cenozoic CO Proxy Integration Project (CenCOPIP) Consortium; Hönisch, B.; Royer, D. L.; et al. The Cenozoic CO_2 Proxy Integration Project ($CenCO_2PIP$) Consortium. Toward a Cenozoic history of atmospheric CO_2. *Science* **2023**, *382*, No. eadi5177, DOI: 10.1126/science.adi5177.

(17) Zhang, Y.; Cao, F.; Song, W.; Jia, X.-F.; Xie, T.; Wu, C.-L.; Yan, P.; Yu, M.; Rauber, M.; Salazar, G.; Szidat, S.; Zhang, Y. Fossil and Nonfossil Sources of Winter Organic Aerosols in the Regional Background Atmosphere of China. *Environ. Sci. Technol.* **2024**, *58*, 1244−1254.

(18) Paradis, S.; Nakajima, K.; van der Voort, T. S.; Gies, H.; Wildberger, A.; Blattmann, T. M.; Broder, L.; Eglinton, T. I. The Modern Ocean Sediment Archive and Inventory of Carbon (MOSAIC): version 2.0. *Earth Syst. Sci. Data* **2023**, *15*, 4105−4125.

(19) Eglinton, T. I.; Eglinton, G. Molecular proxies for paleoclimatology. *Earth Planet. Sci. Lett.* **2008**, *275*, 1−16.

(20) Bao, R.; McNichol, A. P.; Hemingway, J. D.; Lardie Gaylord, M. C.; Eglinton, T. I. Influence of Different Acid Treatments on the Radiocarbon Content Spectrum of Sedimentary Organic Matter Determined by RPO/Accelerator Mass Spectrometry. *Radiocarbon* **2019**, *61*, 395−413.

(21) Wu, W.; Li, H.; Wang, N.; Huo, X.; Zhong, G.; Zhu, L.; Liu, J.; Zhou, Y.; Yan, C.; Bao, R. An approach for carbon content measurement in marine sediment: Application of organic and elemental carbon analyzer. *Mar. Environ. Res.* **2023**, *188*, No. 106000.
(22) Hemingway, J. D.; Rothman, D. H.; Rosengard, S. Z.; Galy, V. V. Technical note: An inverse method to relate organic carbon reactivity to isotope composition from serial oxidation. *Biogeosciences* **2017**, *14*, 5099−5114.
(23) Rosenheim, B. E.; Day, M. B.; Domack, E.; Schrum, H.; Benthien, A.; Hayes, J. M. Antarctic sediment chronology by programmed-temperature pyrolysis: Methodology and data treatment. *Geochem., Geophys., Geosyst.* **2008**, *9*, No. Q04005.
(24) Hemingway, J. D.; Galy, V. V.; Schefuß, E.; Gagnon, A. R.; Dinga, B. J.; Grant, K. E.; Prytherch, J.; Rosengard, S. Z.; McNichol, A. P.; Soulet, G.; Galy, V. V.; Zigah, P. K.; Eglinton, T. I. Assessing the Blank Carbon Contribution, Isotope Mass Balance, and Kinetic Isotope Fractionation of the Ramped Pyrolysis/Oxidation Instrument at NOSAMS. *Radiocarbon* **2017**, *59*, 179−193.
(25) Bao, R.; Strasser, M.; McNichol, A. P.; et al. Tectonically-triggered sediment and carbon export to the Hadal zone. *Nat. Commun.* **2018**, *9*, No. 121.
(26) Boudreau, B. P.; Ruddick, B. R. On a reactive continuum representation of organic matter diagenesis. *Am. J. Sci.* **1991**, *291* (5), 507−538.
(27) He, S.; Yang, H.; Cui, X. Technical note: assessing pretreatment approaches for serial pyrolysis-oxidation analysis of sedimentary organic carbon. *Biogeosciences* **2025**, *22*, 6243−6253.
(28) Maithani, S.; Pradhan, M. Cavity ring-down spectroscopy and its applications to environmental, chemical and biomedical systems. *J. Chem. Sci.* **2020**, *132*, No. 114.
(29) Lin, Y.-C.; Zhang, Y.-L.; Xie, F.; Zhang, W.-Q.; Fan, M.-Y.; Lin, Z. W.; Rella, C. W.; Hoffnagle, J. A. Development of a Monitoring System for Semicontinuous Measurements of Stable Carbon Isotope Ratios in Atmospheric Carbonaceous Aerosols: Optimized Methods and Application to Field Measurements. *Anal. Chem.* **2020**, *92*, 14373−14382.
(30) Flores, E.; Rhoderick, G. C.; Viallon, J.; Moussay, P.; Choteau, T.; Gameson, L.; Guenther, F. R.; Wielgosz, R. I. Methane Standards Made in Whole and Synthetic Air Compared by Cavity Ring Down Spectroscopy and Gas Chromatography with Flame Ionization Detection for Atmospheric Monitoring Applications. *Anal. Chem.* **2015**, *87*, 3272−3279.
(31) Vogel, F. R.; Huang, L.; Ernst, D.; Giroux, L.; Racki, S.; Worthy, D. E. J. Evaluation of a cavity ring-down spectrometer for in situ observations of $^{13}CO_2$. *Atmos. Meas. Tech.* **2013**, *6*, 301−308.
(32) Wang, N.; Li, W.; Liu, X.; Xu, L.; Zhang, X.; Guo, J.; et al. Influences of oxidation ability on precision in nitrogen isotope measurements of organic reference materials using elemental analysis-isotope ratio mass spectrometry. *Rapid Commun. Mass Spectrom.* **2021**, *35*, No. e9122.
(33) Olsen, A.; Lange, N.; Key, R. M.; Tanhua, T.; Bittig, H. C.; Kozyr, A.; Álvarez, M.; Azetsu-Scott, K.; Becker, S.; Brown, P. J.; Carter, B. R.; Cotrim da Cunha, L.; Feely, R. A.; van Heuven, S.; Hoppema, M.; Ishii, M.; Jeansson, E.; Jutterström, S.; Landa, C. S.; Lauvset, S. K.; Michaelis, P.; Murata, A.; Pérez, F. F.; Pfeil, B.; Schirnick, C.; Steinfeldt, R.; Suzuki, T.; Tilbrook, B.; Velo, A.; Wanninkhof, R.; Woosley, R. J. An updated version of the global interior ocean biogeochemical data product, GLODAPv2.2020. *Earth Syst. Sci. Data* **2020**, *12*, 3653−3678.
(34) Liu, J.; Li, Y.; Ding, P.; Xu, B.; Zhang, Y.; Wang, Z.; Liu, D.; Yang, F.; Shen, C.; Chen, Y. Optimizing isolation protocol of organic carbon and elemental carbon for ^{14}C analysis using fine particulate samples. *Atmos. Environ.* **2017**, *154*, 9−19.
(35) Berryman, E. M.; Marshall, J. D.; Rahn, T.; Cook, S. P.; Litvak, M. Adaptation of continuous-flow cavity ring-down spectroscopy for batch analysis of $\delta^{13}C$ of CO_2 and comparison with isotope ratio mass spectrometry. *Rapid Commun. Mass Spectrom.* **2011**, *25*, 2355−2360.
(36) Dickinson, D.; Bodé, S.; Boeckx, P. Measuring ^{13}C-enriched CO_2 in air with a cavity ring-down spectroscopy gas analyser: Evaluation and calibration. *Rapid Commun. Mass Spectrom.* **2017**, *31*, 1892−1902.
(37) Rella, C. W.; Chen, H.; Andrews, A. E.; Filges, A.; Gerbig, C.; Hatakka, J.; Karion, A.; Miles, N. L.; Richardson, S. J.; Steinbacher, M.; Sweeney, C.; Wastine, B.; Zellweger, C. High accuracy measurements of dry mole fractions of carbon dioxide and methane in humid air. *Atmos. Meas. Tech.* **2013**, *6*, 837−860.
(38) Wahl, E. H.; Fidric, B.; Rella, C. W.; Koulikov, S.; Kharlamov, B.; Tan, S.; Kachanov, A. A.; Richman, B. A.; Crosson, E. R.; Paldus, B. A.; Kalaskar, S.; Bowling, D. R. Applications of cavity ring-down spectroscopy to high precision isotope ratio measurement of $^{13}C/^{12}C$ in carbon dioxide. *Isot. Environ. Health Stud.* **2006**, *42*, 21−35.
(39) Dickinson, D.; Bodé, S.; Boeckx, P. System for $\delta^{13}C-CO_2$ and xCO_2 analysis of discrete gas samples by cavity ring-down spectroscopy. *Atmos. Meas. Tech.* **2017**, *10*, 4507−4519.
(40) Hu, L.; Guo, Z.; Feng, J.; Yang, Z.; Fang, M. Distributions and sources of bulk organic matter and aliphatic hydrocarbons in surface sediments of the Bohai Sea, China. *Mar. Chem.* **2009**, *113*, 197−211.
(41) Lim, B.; Cachier, H. Determination of black carbon by chemical oxidation and thermal treatment in recent marine and lake sediments and Cretaceous-Tertiary clays. *Chem. Geol.* **1996**, *131*, 143−154.
(42) Yang, Y.; Chen, F.; Zhang, L.; Liu, J.; Wu, S.; Kang, M. Comprehensive assessment of heavy metal contamination in sediment of the Pearl River Estuary and adjacent shelf. *Mar. Pollut. Bull.* **2012**, *64*, 1947−1955.
(43) O'Keefe, A.; Deacon, D. A. G. Cavity ring-down optical spectrometer for absorption measurements using pulsed laser sources. *Rev. Sci. Instrum.* **1988**, *59*, 2544−2551.
(44) Werle, P.; Mücke, R.; Slemr, F. The limits of signal averaging in atmospheric trace-gas monitoring by tunable diode-laser absorption spectroscopy (TDLAS). *Appl. Phys. B* **1993**, *57*, 131−139.
(45) Crosson, E. R. A cavity ring-down analyzer for measuring atmospheric levels of methane, carbon dioxide, and water vapor. *Appl. Phys. B* **2008**, *92*, 403−408.
(46) Coplen, T. B. Guidelines and recommended terms for expression of stable-isotope-ratio and gas-ratio measurement results. *Rapid Commun. Mass Spectrom.* **2011**, *25*, 2538−2560.
(47) Brand, W. A.; Coplen, T.; Vogl, J.; Rosner, M.; Prohaska, T. Assessment of international reference materials for isotope-ratio analysis (IUPAC Technical Report). *Pure Appl. Chem.* **2014**, *86*, 425−467.
(48) Stoner, S. W.; Schrumpf, M.; Hoyt, A.; Sierra, C. A.; Doetterl, S.; Galy, V.; Trumbore, S. How well does ramped thermal oxidation quantify the age distribution of soil carbon? Assessing thermal stability of physically and chemically fractionated soil organic matter. *Biogeosciences* **2023**, *20*, 3151−3163.
(49) Bao, R.; McIntyre, C.; Zhao, M.; Zhu, C.; Kao, S.-J.; Eglinton, T. I. Widespread dispersal and aging of organic carbon in shallow marginal seas. *Geology* **2016**, *44* (10), 791−794.
(50) Chu, M.; Bao, R.; Strasser, M.; Ikehara, K.; Everest, J.; Maeda, L.; Hochmuth, K.; Xu, L.; McNichol, A.; Bellanova, P.; Rasbury, T.; Kölling, M.; Riedinger, N.; Johnson, J.; Luo, M.; März, C.; Straub, S.; Jitsuno, K.; Brunet, M.; Cai, Z.; Cattaneo, A.; Hsiung, K.; Ishizawa, T.; Itaki, T.; Kanamatsu, T.; Keep, M.; Kioka, A.; McHugh, C.; Micallef, A.; Pandey, D.; Proust, J. N.; Satoguchi, Y.; Sawyer, D.; Seibert, C.; Silver, M.; Virtasalo, J.; Wang, Y.; Wu, T.-W.; Zellers, S. Earthquake-enhanced dissolved carbon cycles in ultra-deep ocean sediments. *Nat. Commun.* **2023**, *14* (1), No. 5427.
(51) Schwestermann, T.; Eglinton, T. I.; Haghipour, N.; McNichol, A. P.; Ikehara, K.; Strasser, M. Event-dominated transport, provenance, and burial of organic carbon in the Japan Trench. *Earth Planet. Sci. Lett.* **2021**, *563*, No. 116870.
(52) Hayes, J. M.; Strauss, H.; Kaufman, A. J. The abundance of ^{13}C in marine organic matter and isotopic fractionation in the global biogeochemical cycle of carbon during the past 800 Ma. *Chem. Geol.* **1999**, *161*, 103−125.
(53) Zhu, Q.-Z.; Yin, X.; Taubner, H.; Wendt, J.; Friedrich, M. W.; Elvert, M.; Hinrichs, K.-U.; Middelburg, J. J. Secondary production and priming reshape the organic matter composition in marine sediments. *Sci. Adv.* **2024**, *10*, No. eadm8096.

https://doi.org/10.1021/acs.analchem.6c00100
Anal. Chem. XXXX, XXX, XXX−XXX

(54) Freeman, E. C.; Emilson, E. J. S.; Dittmar, T.; Braga, L. P. P.; Emilson, C. E.; Goldhammer, T.; Martineau, C.; Singer, G.; Tanentzap, A. J. Universal microbial reworking of dissolved organic matter along environmental gradients. *Nat. Commun.* **2024**, *15*, No. 187.
(55) Fernandez, A.; Santos, G. M.; Williams, E. K.; Pendergraft, M. A.; Vetter, L.; Rosenheim, B. E. Blank Corrections for Ramped Pyrolysis Radiocarbon Dating of Sedimentary and Soil Organic Carbon. *Anal. Chem.* **2014**, *86*, 12085−12092.
(56) O'Connor, J. A.; Lu, K.; Guo, L.; Rosenheim, B. E.; Liu, Z. Composition and lability of riverine dissolved organic matter: Insights from thermal slicing ramped pyrolysis GC−MS, amino acid, and stable isotope analyses. *Org. Geochem.* **2020**, *149*, No. 104100.
(57) Eglinton, T. I.; Benitez-Nelson, B. C.; Aluwihare, L. I.; Pearson, A.; Bauer, J. E.; McNichol, A. P.; Druffel, E. R. M.; Bauer, J. E.; McNichol, A. P. Variability in Radiocarbon Ages of Individual Organic Compounds from Marine Sediments. *Science* **1997**, *277*, 796−799.
(58) LaRowe, D. E.; Arndt, S.; Bradley, J. A.; Estes, E. R.; Hoarfrost, A.; Lang, S. Q.; Lloyd, K. G.; Maignien, L.; Mahmoudi, N.; Orsi, W. D.; Walter, S. R. S.; Steen, A. D. The fate of organic carbon in marine sediments - New insights from recent data and analysis. *Earth-Sci. Rev.* **2020**, *204*, No. 103146.
(59) Arndt, S.; Jørgensen, B. B.; LaRowe, D. E.; Middelburg, J. J.; Pancost, R. D.; Regnier, P. Quantifying the degradation of organic matter in marine sediments: A review and synthesis. *Earth-Sci. Rev.* **2013**, *123*, 53−86.
(60) Biddle, J. F.; Lipp, J. S.; Lever, M. A.; Lloyd, K. G.; Sørensen, K. B.; Anderson, R.; Fredricks, H. F.; Elvert, M.; Kelly, T. J.; Schrag, D. P.; Sogin, M. L.; Brenchley, J. E.; Teske, A.; House, C. H.; Hinrichs, K.-U. Heterotrophic Archaea dominate sedimentary subsurface ecosystems off Peru. *Proc. Natl. Acad. Sci. U.S.A.* **2006**, *103*, 3846−3851.
(61) Morono, Y.; Terada, T.; Nishizawa, M.; Ito, M.; Hillion, F.; Takahata, N.; Sano, Y.; Inagaki, F. Carbon and nitrogen assimilation in deep subseafloor microbial cells. *Proc. Natl. Acad. Sci. U.S.A.* **2011**, *108*, 18295−18300.
(62) Galy, V.; France-Lanord, C.; Beyssac, O.; Faure, P.; Kudrass, H.; Palhol, F. Efficient organic carbon burial in the Bengal fan sustained by the Himalayan erosional system. *Nature* **2007**, *450*, 407−410.
(63) Wagner, S.; Jaffé, R.; Cawley, K. M.; Dittmar, T.; Stubbins, A.; et al. Isotopic composition of oceanic dissolved black carbon reveals non-riverine source. *Nat. Commun.* **2019**, *10*, No. 5064.
(64) Sanderman, J.; Grandy, A. S. Ramped thermal analysis for isolating biologically meaningful soil organic matter fractions with distinct residence times. *Soil* **2020**, *6*, 131−144.
(65) Guo, J.; Yuan, H.; Song, J.; Li, X.; Duan, L.; Li, N.; Wang, Y. Evaluation of Sedimentary Organic Carbon Reactivity and Burial in the Eastern China Marginal Seas. *J. Geophys. Res.: Oceans* **2021**, *126* (4), No. e2021JC017207.
(66) Cao, Y.; Bi, R.; Wang, X.; Chen, X.; Hu, J.; Wang, Y.; Jiang, Y.; Zhang, H.; Xing, L.; Zhao, M. The Sources and Burial of Marine Organic Carbon in the Eastern China Marginal Seas. *Front. Mar. Sci.* **2022**, *9*, No. 824181.
(67) Li, H.; Lin, D.; Zhang, H.; Wang, N.; Zhou, Y.; Wu, W.; Liu, J.; Che, Y.; Xia, C.; Zhu, L.; Peng, C.; Liu, Q.; He, Q.; Bao, R. Preservation of Organic Carbon Associated with Iron on Continental Shelves Influenced by Hydrodynamic Processes. *Environ. Sci. Technol.* **2024**, *58* (33), 14698−14708.



https://doi.org/10.1021/acs.analchem.6c00100
Anal. Chem. XXXX, XXX, XXX−XXX